Atmos. Chem. Phys. Discuss., doi:10.5194/acp-2016-449, 2016
Manuscript under review for journal Atmos. Chem. Phys.
Published: 8 July 2016

Atmospheric Chemistry and Physics Discussions

A mid-latitude stratosphere dynamical index for attribution of stratospheric variability and improved ozone and temperature trend analysis

William T. Ball[1,2], Aleš Kuchař[3], Eugene V. Rozanov[1,2], Johannes Staehelin[1], Fiona Tummon[1], Anne K. Smith[4], Timofei Sukhodolov[1,2], Andrea Stenke[1], Laura Revell[1,5], Ancelin Coulon[1], Werner Schmutz[2], and Thomas Peter[1]

[1]Institute for Atmospheric and Climate Science, Swiss Federal Institute of Technology Zurich, Universitaetstrasse 16, CHN, CH-8092 Zurich, Switzerland
[2]Physikalisch-Meteorologisches Observatorium Davos World Radiation Centre, Dorfstrasse 33, 7260 Davos Dorf, Switzerland
[3]Department of Atmospheric Physics, Faculty of Mathematics and Physics, Charles University in Prague, V Holesovickach 2, 180 00 Prague 8, Czech Republic
[4]National Center for Atmospheric Research, Boulder, Colorado
[5]Bodeker Scientific, Alexandra, New Zealand

Correspondence to: W. T. Ball (william.ball@env.ethz.ch)

Abstract. We find that wintertime temperature anomalies near 4 hPa and 50°N/S are related, through dynamics, to anomalies in ozone and temperature, particularly in the tropical stratosphere, but also throughout the upper stratosphere and mesosphere. These mid-latitude anomalies occur on timescales of up to a month, and are related to changes in wave-forcing. A change in the meridional circulation extends from the middle stratosphere into the mesosphere and forms a temperature-change quadrupole from equator to pole. We develop a dynamical index based on detrended, deseasonalised mid-latitude temperature. When employed in multiple linear regression, this index can account for up to 40% of the total variability of temperature and ozone and a doubling of the total coefficient of determination in the equatorial stratosphere above 20 hPa. Further, the uncertainty on all multiple-linear regression coefficients can be reduced by up to 45% and 25% in temperature and ozone, respectively, and so this index is an important tool for quantifying current and future ozone recovery.

1 Introduction

Trend analysis, typically using multiple linear regression (MLR), is a key approach to understand drivers of long-term changes in the stratosphere (e.g. WMO (1994), Soukharev and Hood (2006), Chiodo et al. (2014), Kuchar et al. (2015), Harris et al. (2015)). Ozone and temperature have received most attention, partly because they have the longest observational records. Temperature is important for understanding climate change, while quantifying changes in the ozone layer is necessary to estimate future impacts of elevated, or reduced, ultraviolet (UV) radiation reaching the surface, especially following the implementation of the Montreal Protocol to reduce halogen-containing ozone depleting substances (HODSs) damaging the ozone layer.

Atmos. Chem. Phys. Discuss., doi:10.5194/acp-2016-449, 2016
Manuscript under review for journal Atmos. Chem. Phys.
Published: 8 July 2016

Atmospheric Chemistry and Physics Discussions

In MLR analysis, stratospheric variability is usually described with six regressors that represent the solar cycle UV flux changes (e.g., with the F10.7cm radio flux), volcanic eruptions (stratospheric aerosol optical depth; SAOD), the El Nino Southern Oscillation (ENSO) surface temperature variations, two orthogonal modes of the dynamical quasi-biennial oscillation (QBO), and the equivalent effective stratospheric chlorine (EESC), which describes the long-term influence of HODSs on ozone concentration and temperature.

Ozone and temperature variations in the stratosphere are directly modulated by changes in solar flux, particularly in the UV (see e.g. (Haigh et al., 2010; Ball et al., 2016) and references therein). Ozone concentration also responds to changes in the Brewer-Dobson circulation (BDC), whereby air rises in the tropics, advects polewards either on a lower, shallow- (below $\sim$50 hPa) or an upper, deep-branch, and descends at mid-latitudes (less than $\sim$60°) or over the poles, respectively (Birner and Bönisch, 2011). The BDC is mainly driven by mid-latitude upward propagating planetary and gravity waves that break and impart momentum, acting like a paddle to drive the circulation (Haynes et al., 1991; Holton et al., 1995; Butchart, 2014). Wave forcing depends on the mean-state of the flow, and vice-versa (Charney and Drazin, 1961; Holton and Mass, 1976); changes in either affect ozone transport by a change in the speed of the BDC that leads to adiabatic heating, or cooling, and directly affects chemistry through temperature-dependent reaction rates (Chen et al., 2003; García-Herrera et al., 2006; Shepherd et al., 2007; Lima et al., 2012). As such, ozone and temperature have an inverse relationship in the equatorial stratosphere, which in turn has a dependence on dynamics (Stolarski et al., 2012), although this is not always the case in the lower stratosphere (Zubov et al., 2013). Ultimately, then, dynamical perturbations at mid-to-high latitudes can directly influence the variability of ozone and temperature (Sridharan et al., 2012; Nath and Sridharan, 2015).

The stratospheric ozone layer has been damaged by the use of HODSs and following a ban through the 1987 Montreal Protocol (Solomon, 1999), levels of HODSs have declined since their peak in 1998 (Egorova et al., 2013; Chipperfield et al., 2015). However, the rate of ozone recovery is latitude dependent, with southern mid-to-high latitudes expected to recover by the end of the century, and northern regions by mid-century (WMO, 2011). The increase in ozone comes partly from HODS reductions, but also because the BDC is expected to accelerate (Garcia and Randel, 2008), which reduces the time for ozone depletion to occur, leads to faster transport of ozone out of the equatorial region, and therefore a reduction of ozone over the equator and a prevention of a full recovery over the tropics. Additionally, the cooling stratosphere will slow ozone depletion in the gas phase with the result in the mid-latitudes of a 'super-recovery' (WMO, 2014). However, estimates of ozone trends from 1998 have a high level of uncertainty (Harris et al., 2015) because various long-term datasets provide different pictures (Tummon et al., 2015), and we do not understand much of the stratospheric variability on short-timescales. Anomalous, monthly variability, like that at the equator as shown in Figs. 7 and 8 in Shapiro et al. (2013), and which could be related to high latitude variability (e.g. Kuroda and Kodera (2001) and Hitchcock et al. (2013)) may simply be considered as noise in MLR trend estimates (and other regressors) where it is not accounted for, which increases the uncertainty.

Our aim here is to provide an index (section 4) to account for sporadic, noise-like stratospheric variability in monthly timeseries and, therefore, improve estimates of trend and regressor variability, and reduce their uncertainties (section 5). We do this using model, reanalysis and observational data (section 2) to identify a source for the short-term variability (section 3).

Atmos. Chem. Phys. Discuss., doi:10.5194/acp-2016-449, 2016
Manuscript under review for journal Atmos. Chem. Phys.
Published: 8 July 2016

Atmospheric Chemistry and Physics Discussions

2 Data and models

2.1 Chemsitry climate model in specified dynamics mode

To investigate temperature and ozone variability in the stratosphere and mesosphere at all latitudes, without data gaps, we simulate historical ozone and temperature variations using the Chemistry Climate Model (CCM) SOlar Climate Ozone Links (SOCOL; version 3 (Stenke et al., 2013)) in specified dynamics mode, whereby the vorticity and divergence of the wind fields, temperature and the logarithm of surface pressure are 'nudged' using the ERA-Interim reanalysis (Dee et al., 2011) between 1983–2012 and up to 0.01 hPa; see Ball et al. (2016) for full nudging details. Note that we use the Stratospheric Processes and their Role in Climate (SPARC) International Global Atmospheric Chemistry (IGAC) Chemistry Climate Model Intercomparison (CCMI) boundary conditions and external forcings, except for the solar irradiance input, for which we use the SATIRE-S model (Krivova et al., 2003; Yeo et al., 2014). In the following we focus on temperature and ozone variables; the former is nudged, while the latter is simulated by the CCM SOCOL model.

2.2 Observations

We verify that the nudged-model output fields ozone (not nudged) and temperature (nudged) agree with observations. For ozone we use the Stratospheric Water and OzOne Satellite Homogenized (SWOOSH) ozone composite (Davis et al., 2016) for 215–0.2 hPa (∼10–55 km) and 1979–2012 at all latitudes. For temperature, we compare the nudged-model output with independent measurements from the Sounding of the Atmosphere using Broadband Emission Radiometry (SABER) instrument (Russell et al., 1999) on the Thermosphere-Ionosphere-Mesosphere-Energetics and Dynamics (TIMED) satellite, spanning 2002–2015 and for 100 to 0.00001 hPa (∼10–140 km) and latitudes out to 52°.

For the MLR analysis (section 5) we additionally consider equatorial ozone from the Global OZone Chemistry And Related trace gas Data records for the Stratosphere (GOZCARDS; Froidevaux et al. (2015)), Solar Backscatter Ultraviolet Instrument Merged Cohesive (SBUV-Mer.; Wild and Long (2016)), SBUV Merged Ozone Dataset (SBUV-MOD; Frith et al. (2014)) composites and temperature from the Stratospheric Sounding Unit (SSU; Zou et al. (2014)) observations and JRA-55 (Ebita et al., 2011) and MERRA (Rienecker et al., 2011) reanalyses. All observations are re-gridded onto the SOCOL model pressure levels and latitudes and consider monthly mean zonally-averaged data.

3 Anomalous dynamical variability

3.1 Equatorial ozone and temperature variability

To identify short-term, 'anomalous' variability distinct from behaviour on seasonal and longer timescales, we remove all long-term variability by smoothing each latitude-pressure time series with a 13-month running mean, and then deseasonalise monthly values. We apply this pre-processing to all variables in sections 3 and 4. An example nudged equatorial (20°S–20°N) ozone and temperature anomaly time series from the CCM SOCOL model at 2.5 hPa is shown in Fig. 1. SWOOSH ozone

Atmos. Chem. Phys. Discuss., doi:10.5194/acp-2016-449, 2016
Manuscript under review for journal Atmos. Chem. Phys.
Published: 8 July 2016

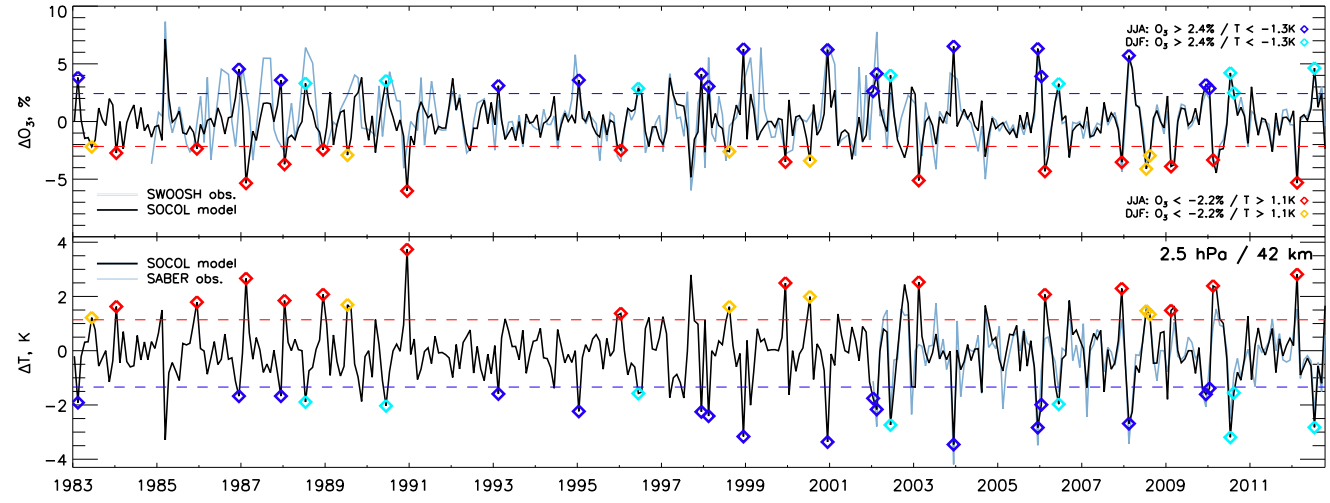

Figure 1. Monthly anomalies of equatorial (20°S–20°N) ozone (upper; %) and temperature (lower; degrees Kelvin) at 2.5 hPa, following the subtraction of 13-month box-car smoothing and monthly-deseasonalising from the CCM SOCOL model in specified dynamics mode. SWOOSH ozone composite time series and SABER temperature measurements are shown in light-blue in the upper and lower plots, respectively. The dashed blue and red horizontal lines are the thresholds shown in Fig. 2. June-July-August (JJA) anomalies exceeding the thresholds have orange (high-T) and turquoise (low-T) diamonds; December-January-February (DJF) anomalies are identified by red (high-T) and blue (low-T) diamonds.

from 1985 to 2012, and SABER temperature from 2002 to 2012 (Fig. 1), show similar anomalous behaviour to the model and have correlation coefficients (r_c) of 0.72 and 0.83 with the nudged model results, respectively; the model, therefore, reproduces observations well. The monthly temperature and ozone anomalies have a very strong relationship, especially between 0.1 and 6.3 hPa, with negative r_c reaching -0.95 (Fig. 2) between 0.1 and 10 hPa, while being positive elsewhere.

To establish the coherency of the ozone-temperature relationship in the tropics, we identify 'extreme' anomalies (or 'events') as those at least at the 90th percentile from the mean in temperature and ozone at less than the 10th percentile (and vice versa). We call 'low-T' events those that have low equatorial temperature at the same time as a high ozone concentration (blue lines at 2.5 hPa, Fig. 2), and 'high-T' for the opposite situation (red lines). We note that for reference the ozone concentration maximum is at ∼10 hPa. We use 2.5 hPa as a reference here, but other pressure levels at altitudes between 0.1 and 6 hPa give similar results. The majority of the events (45/60) occur in December-January-February (DJF; red/blue in Fig. 2) and June-July-August (JJA) (yellow/turquoise in Fig. 2). High-T and low-T months remain grouped, but mix and lose coherence at altitudes below 10 hPa, implying that the events have a similar source at all altitudes above 10 hPa, but a different one below (i.e. r_c is high at 25 and 40 hPa, but the events at 25 hPa are well-mixed). This indicates a likely transition between BDC branches and that the driver of variability is dynamical, which we confirm in the following.

Atmos. Chem. Phys. Discuss., doi:10.5194/acp-2016-449, 2016
Manuscript under review for journal Atmos. Chem. Phys.
Published: 8 July 2016

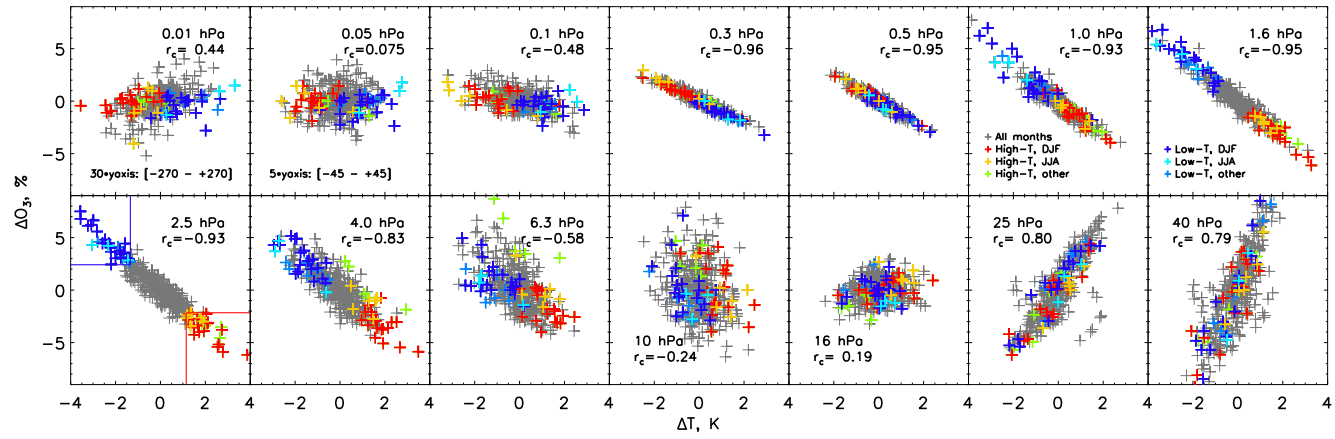

Figure 2. (**left**) Regression of equatorial (20N–20S) ozone and temperature anomalies (following 13-month smoothing and monthly deseasonalising) from the CCM SOCOL model in specified dynamics mode for pressure levels 0.01 to 40 hPa (∼80 – 22 km). Grey crosses are for all months in 1983/01–2012/10. Coloured crosses in each plot are determined at 2.5 hPa (lower-left) by those within regions defined by the red (high-T events) and blue lines (low-T events); red crosses are for high-T events in December, January, and February (DJF), yellow for high-T events in June, July and August (JJA), and green for 'other' high-T events. Dark blue, turquoise and blue represent DJF, JJA and 'other' low-T months (see also legends in 1.0 and 1.6 hPa plots). Correlation coefficients are given for the grey crosses. The y-scale is different at 0.01 and 0.05 hPa, as indicated in the plots.

3.2 Mid-latitude temperature variability

To identify and locate the source of the driver behind the ozone and temperature anomalies shown and described in the previous section, in Fig. 3 we correlate the 2.5 hPa equatorial temperature low-T and high-T events with detrended and deseasonalised temperature at all latitudes and pressure-levels, for DJF and JJA months (Figs. 3a and b, respectively). A quadrupole-like structure emerges with positive correlations centred around 2.5 hPa at the equator and in the winter-polar mesosphere (<0.8 hPa), and negative correlations in the winter stratospheric mid-to-high-latitudes and the equatorial mesosphere. The inverse correlation in the stratosphere for DJF extreme months peaks at ∼52°N (r_c= -0.92); JJA events peak at ∼43°S (r_c= -0.93). We find similar results when using other equatorial pressure levels near 2.5 hPa as a reference to calculate correlations.

Figures 3c–f are temperature composites for each event type: (c) DJF Low-T, (d) JJA Low-T, (e) DJF High-T and (f) JJA High-T; all show the same temperature-quadrupole structure as in Fig. 3a–b (up to the sign; signals at two and three standard deviations from zero are given as yellow and blue contours, respectively). Equatorial temperature anomalies (∼2 K) are smaller than at high latitudes (∼5 K or more). The peak temperature response at mid-to-high latitudes does not always reside at the same location as the peak correlation. The quadrupole structure is also evident in SABER observations (Fig. 4), though the statistics are less robust since the period is shorter. Thus, we can be confident that the nudged-model is giving a good representation of observations.

Atmos. Chem. Phys. Discuss., doi:10.5194/acp-2016-449, 2016
Manuscript under review for journal Atmos. Chem. Phys.
Published: 8 July 2016

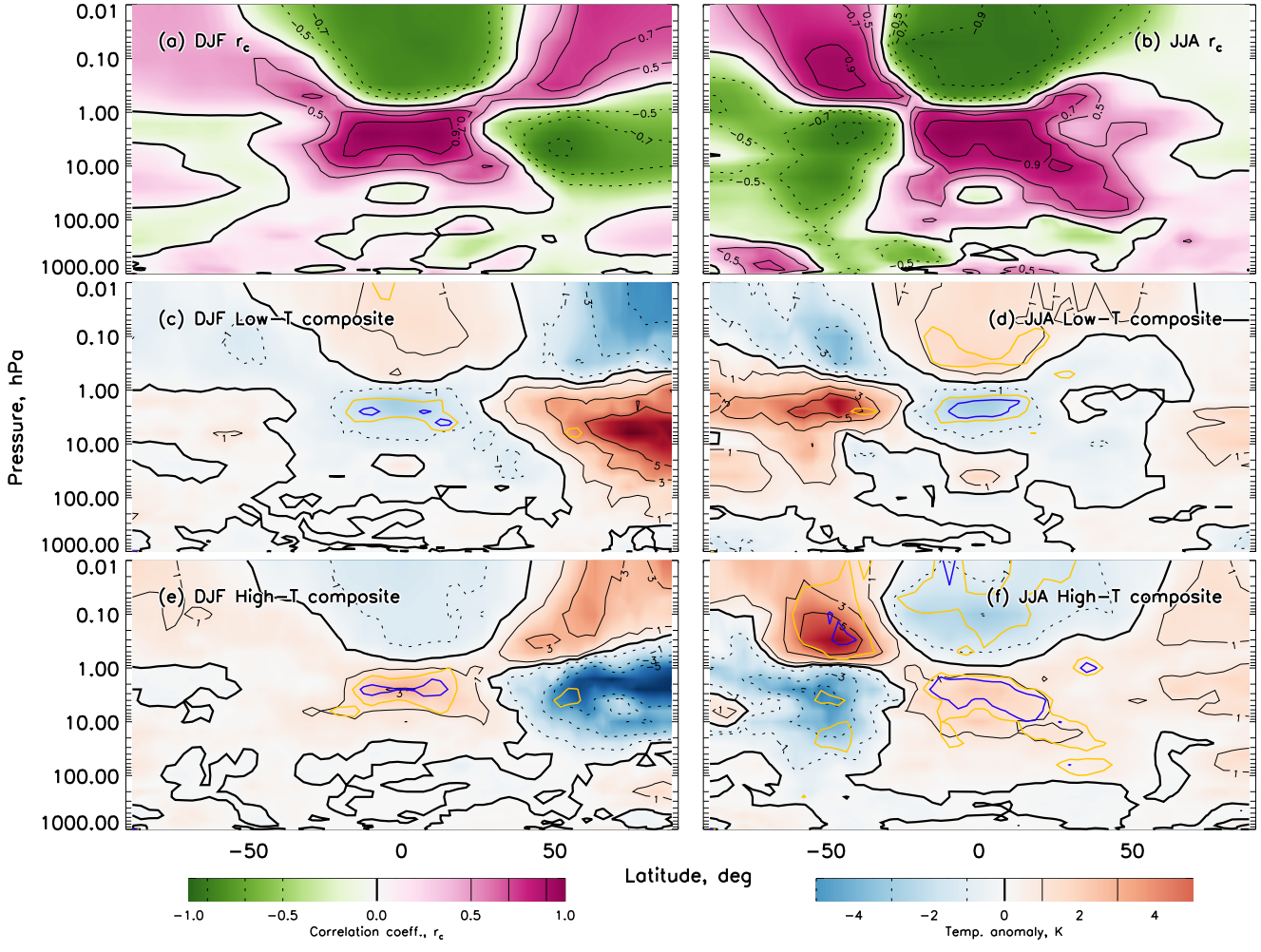

Figure 3. Correlation coefficient maps of zonal mean 20N–20S 2.5 hPa temperature anomalies from the SOCOL model with respect to latitude and altitude for all identified low- and high-T (a) DJF and (b) JJA events, as defined in Fig. 2. (**c–f**) Composite temperatures for (c) DJF low-T, (d) JJA low-T, (e) DJF high-T and (f) JJA high-T events. Dashed (solid) contours are negative (positive) with the bold line representing zero. Signals at the 2 and 3 standard deviations from zero are given as yellow and blue contours, respectively, in panels c–f.

The quadrupole structure is likely the result of (i) an acceleration of the BDC that adiabatically cools the equator during Low-T events as more air arrives at high-latitudes, and adiabatically heats there, and (ii) an deceleration of the BDC that adiabatically heats the equator during High-T events as less air arrives at high-latitudes leading to cooling there; both processes are associated with changes in wave-activity.

We show that the mid-latitude temperature, and equatorial temperature and ozone, anomalies are related to variations in wave activity using the Transformed Eulerian Mean streamfunction (TEMS; Figs. 5), a measure of the mass flux (positive values imply clockwise flow along contours, negative anti-clockwise) and the Eliassen-Palm Flux divergence (EPFD; Figs. 6),

Atmos. Chem. Phys. Discuss., doi:10.5194/acp-2016-449, 2016
Manuscript under review for journal Atmos. Chem. Phys.
Published: 8 July 2016

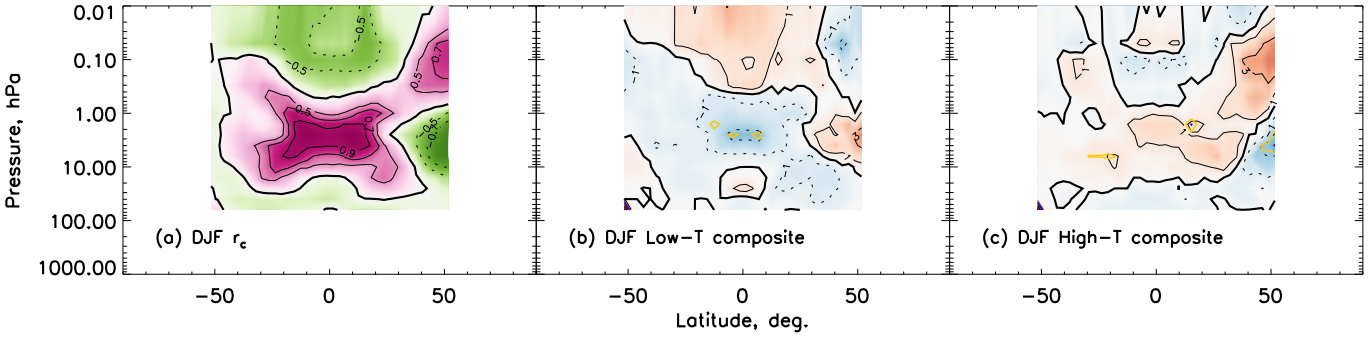

Figure 4. (**a**) SABER temperature data correlation coefficient map of zonal mean 20N–20S 2.5 hPa anomalies with all latitudes and altitudes for all low- and high-T DJF and events. Composite temperatures for DJF (**b**) low-T and (**c**) high-T events, as defined in Fig 2. Shading colours and black contours are the same as in Fig. 3 (dashed, negative; solid, positive; thick, zero). Signals at two standard deviations from zero are given as purple contours in panels b and c.

which is a measure of the resolved wave-induced forcing of the mean flow (positive values imply an acceleration of the zonal mean flow and a deceleration of the BDC, and negative values the opposite). Using the events identified in Figs. 1 and 2, and used in Fig. 3, we find clear EPFD and TEMS anomalies centred near 55°, slightly poleward of the mid-high-latitude peak correlations (Fig. 3a–b). As anomalies, they do not represent a reversal of meridional air flow, but a slowing or acceleration. When high-T anomalies occur the EPFD is positive, which implies zonal mean westerly winds have accelerated and the BDC has slowed, which is confirmed by the TEMS, indicating increased equatorward flow. This will have exact effect found, of adiabaticly heating the equatorial region and cooling the mid-to-high latitudes relative to the mean state. The opposite is the case for low-T anomalies. These results confirm that equatorial anomalies are dynamically driven. The consequence of the circulation changes for ozone is that a temperature increase leads to faster catalytic destruction, and therefore a decrease of ozone, and vice versa for temperature decreases, exactly as we see.

4 Mid-latitude stratosphere dynamical (MLSD) index

The link between anomalous mid-latitude temperature changes and equatorial temperature and ozone provides a way to account for sporadic variability. When performing, e.g., an MLR analysis to understand variability in the stratosphere, such an index of monthly, anomalous variability can account for a large proportion of variability previously unaccounted for, and drive down uncertainties on regressor estimates. We focus here on the equatorial region, and while we did not perform any tests, our results imply this index could be applied to other locations in the stratosphere and mesosphere.

Below, we describe how we construct a mid-latitude stratosphere dynamical (MLSD) index based upon detrended and deseasonalised temperature averaged over 43–49°S and 2.5–6.3 hPa for June–October months, and averaged over 52–57°N and 4–10 hPa for November–May months. Our index utilizes the output from CCM SOCOL in specified dynamics mode, similar to ERA-Interim and observations, but such an index could be constructed in a similar way for a specific model output.

Atmos. Chem. Phys. Discuss., doi:10.5194/acp-2016-449, 2016
Manuscript under review for journal Atmos. Chem. Phys.
Published: 8 July 2016

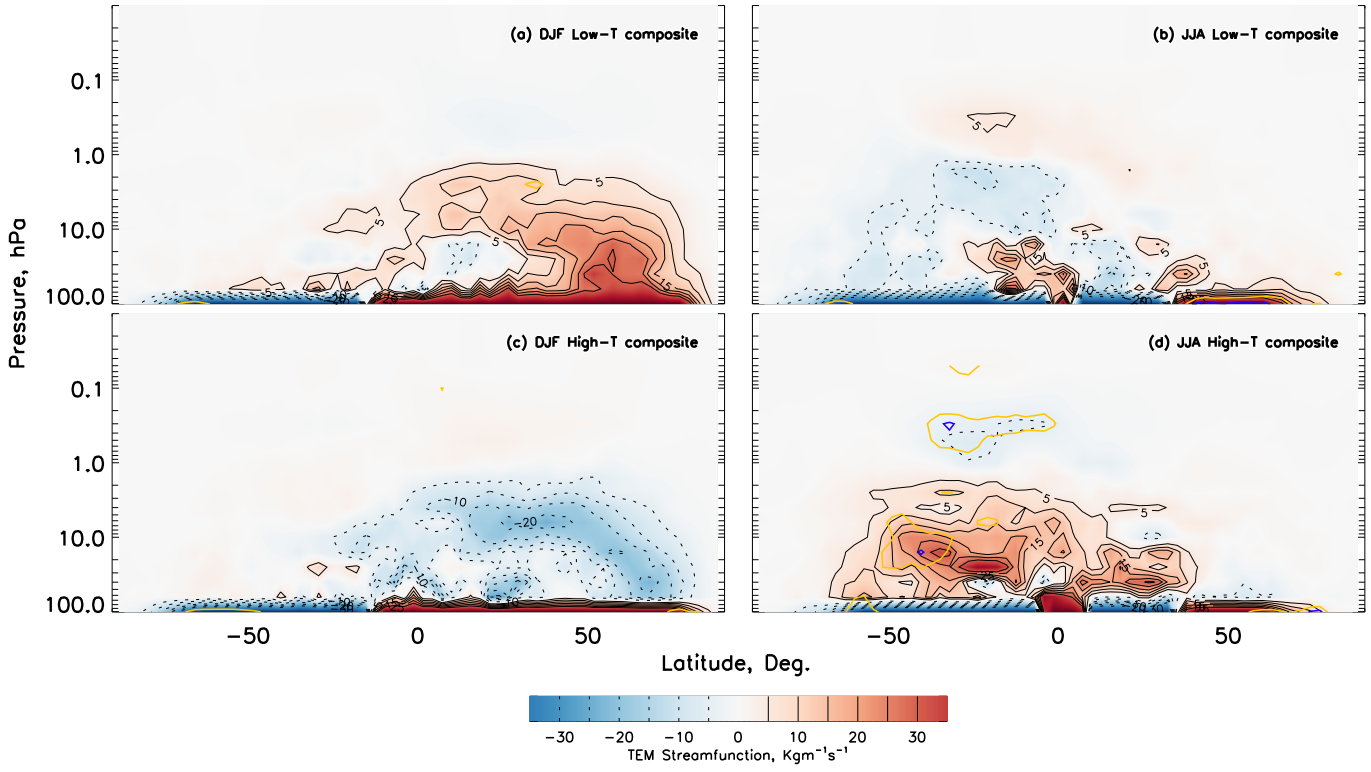

Figure 5. The median of the Transformed Eulerian Mean streamfunction (TEMS) anomalies for (a) DJF Low-Temperature events, (b) DJF High-T events, (c) JJA Low-T events, (d) JJA High-T events for the same months as in Fig. 3c–f. Contours lines (solid, positive; dashed negative) and colours are given in the legend. Positive values indicate clockwise-acceleration along the contour lines; negative are anti-clockwise. Data are from the SOCOL model in specified dynamics mode.

4.1 Construction

To construct a mid-latitude stratosphere dynamical (MLSD) index requires the identification of maximum correlation, or explanatory power, between the equator and each hemisphere, and then the combination of these. While we have previously considered just the extreme events, we now consider all monthly anomalies between 1983 and 2012. While wave-activity drives the temperature changes, it is not an easily observable quantity. Thus, temperature is a natural and simple quantity to build the index with. Additionally, we have found that the CCM SOCOL model in free-running mode (i.e. without nudging) shows the same anomalous temperature-quadrupole structure as in Fig. 3. Therefore, one can easily construct an index using model data to represent anomalous behaviour in the equatorial regions, and elsewhere where there is a quadrupole response.

We identify the maximum inverse temperature correlations at mid-latitudes in both December-January-February (DJF) and June-July-August (JJA) by varying the reference equatorial pressure-level. We find that averaging over the nine grid-cells centred on the mid-latitude peak improves the relationship with the equatorial region. Therefore, we construct the index with

Atmos. Chem. Phys. Discuss., doi:10.5194/acp-2016-449, 2016
Manuscript under review for journal Atmos. Chem. Phys.
Published: 8 July 2016

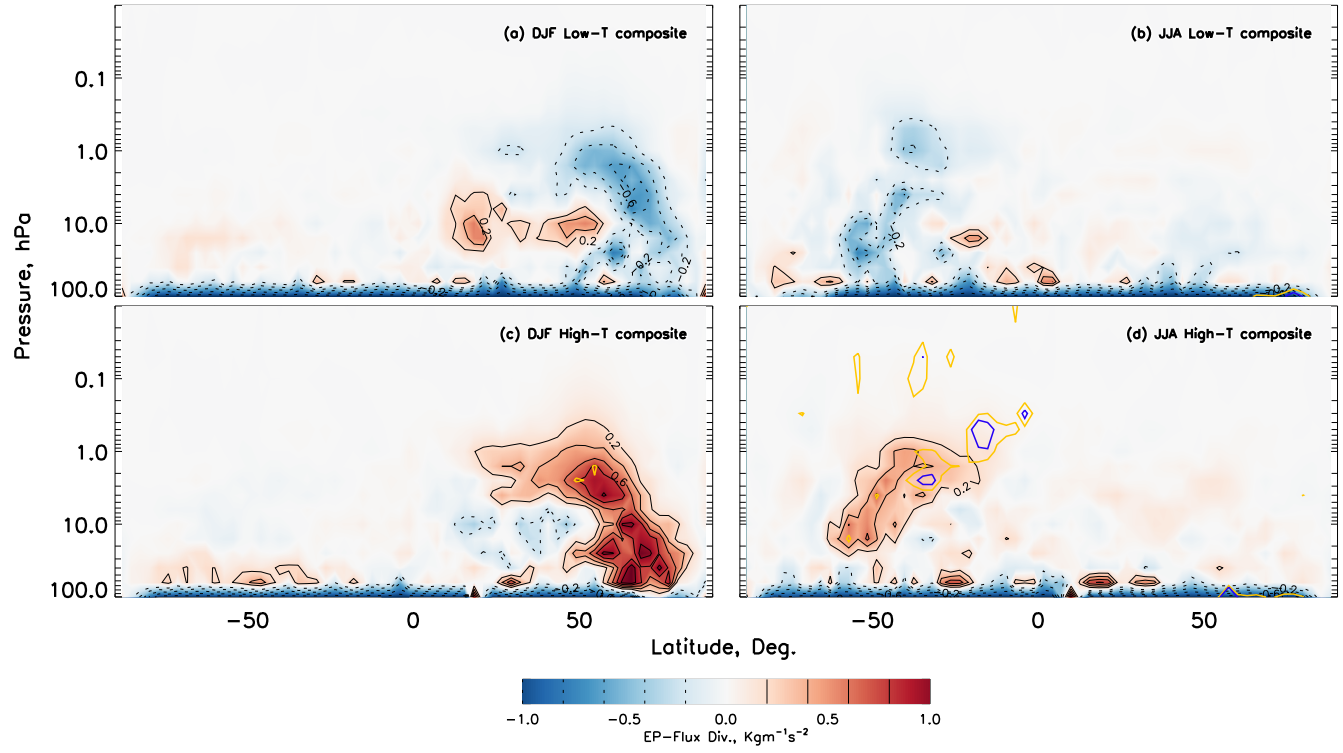

Figure 6. As for Fig. 5, but for EP-Flux Divergence. Positive values indicate increased wave-activity; negative, decreased activity.

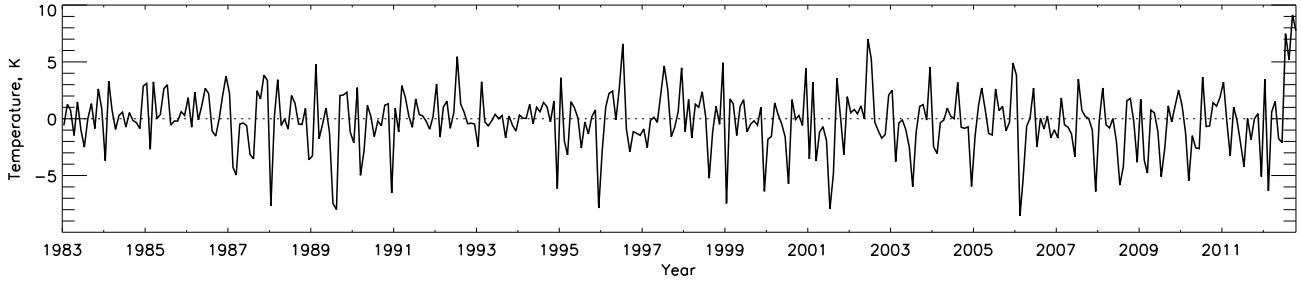

Figure 7. The MLSD index from the CCM SOCOL model in specifed dynamics mode using ERA-Interim from 1983 to 2012.

anomalous temperatures averaged over 43–49°S and 2.5–6.3 hPa in the southern hemisphere (SH) JJA months, and 52–57°N and 4–10 hPa in the northern hemisphere (NH) DJF months.

For March–May and September–November months, we complete the MLSD index by combining November–April NH anomalies with May–October SH anomalies; this combination maximises the relationship with equatorial temperature. We plot the index derived from the CCM SOCOL model in specifed dynamics mode using ERA-Interim in Fig. 7. Fig. 8 shows the SH and NH mid-latitude temperature anomalies verses the 4 hPa 20S–20N equatorial average (a and b, respectively;

Atmos. Chem. Phys. Discuss., doi:10.5194/acp-2016-449, 2016
Manuscript under review for journal Atmos. Chem. Phys.
Published: 8 July 2016

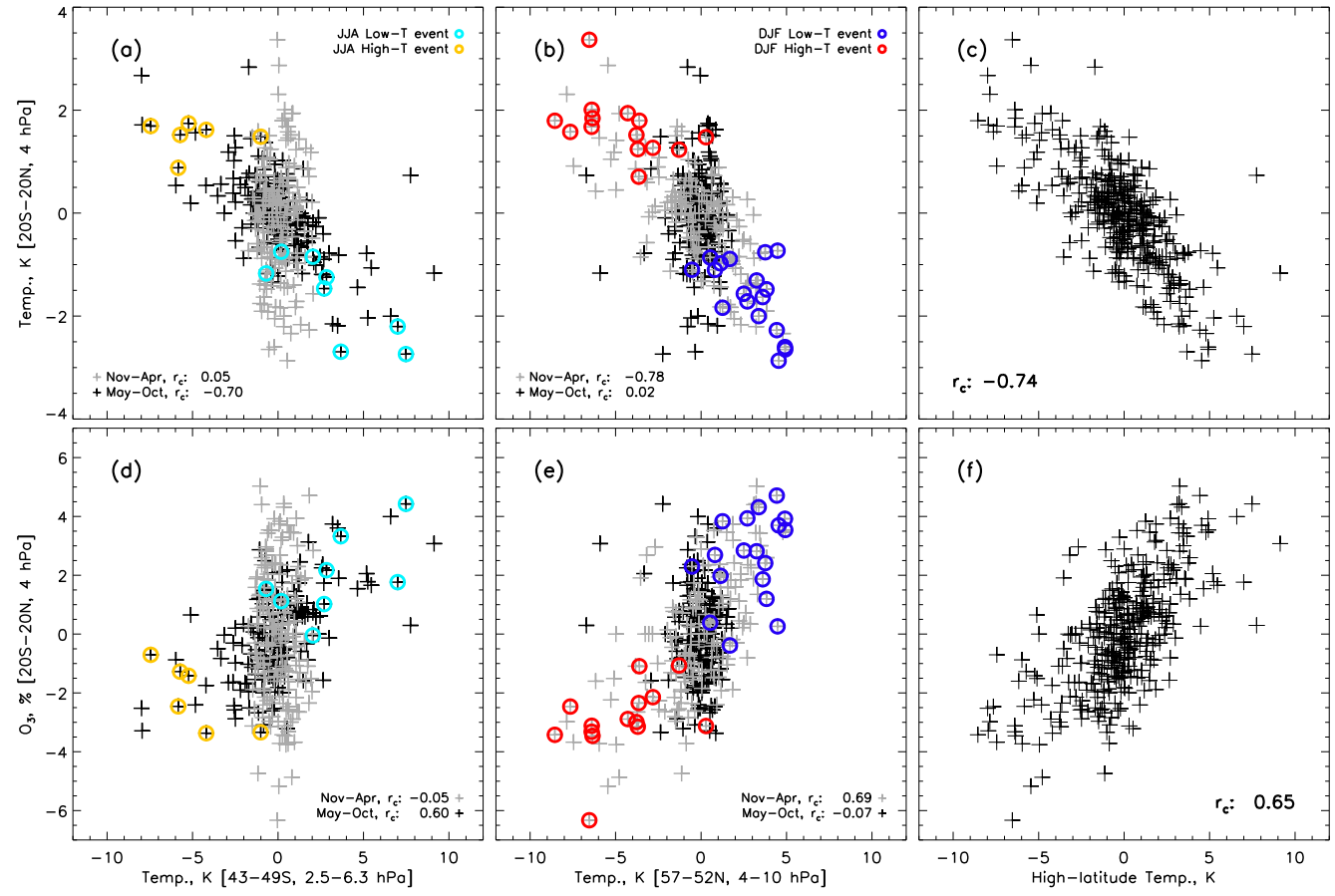

Figure 8. (**a–b**) SOCOL equatorial temperature anomalies (4hPa, 20N–20S) plotted against (a) temperature means from 2.5–6.3 hPa and 43–49S and (b) 52–57N and 4–10 hPa. (**d–e**) As for upper panels, but equatorial ozone anomalies (4 hPa, 20N–20S) are instead plotted against high-latitude temperature anomalies. Grey crosses are for November–April months; black crosses for May–October; correlations for both periods are given in each panel. Red and blue circles identify the DJF High-T and Low-T events in Fig. 2, respectively; orange and light-blue circles similarly identify JJA events. (**c,f**) May–October 43–49S temperatures and November-April 52–57N temperatures are combined in the right panel (MLSD index) and plotted against equatorial (c) temperature and (f) ozone.

grey crosses represent November–April months, and black May–October). The SH May–October temperature anomalies are inversely correlated with equatorial temperatures (r_c=-0.70) while November–April are not (r_c=0.05); the opposite is true for the NH (r_c=0.02 and -0.78, respectively). The ozone-temperature events identified in Fig. 1 are highlighted with coloured circles, showing that the equatorial anomalies are related to mid-latitude wave-driving. Fig. 8c shows the MLSD index plotted against all equatorial temperature anomalies at 4 hPa (r_c=-0.74). The lower panels (d–f) show the equatorial ozone relationship with respect to mid-latitude temperature and the MLSD index; the absolute correlation coefficient is lower (r_c=0.65) than for equatorial temperature in the upper panels, but there is still a strong relationship.

Atmos. Chem. Phys. Discuss., doi:10.5194/acp-2016-449, 2016
Manuscript under review for journal Atmos. Chem. Phys.
Published: 8 July 2016

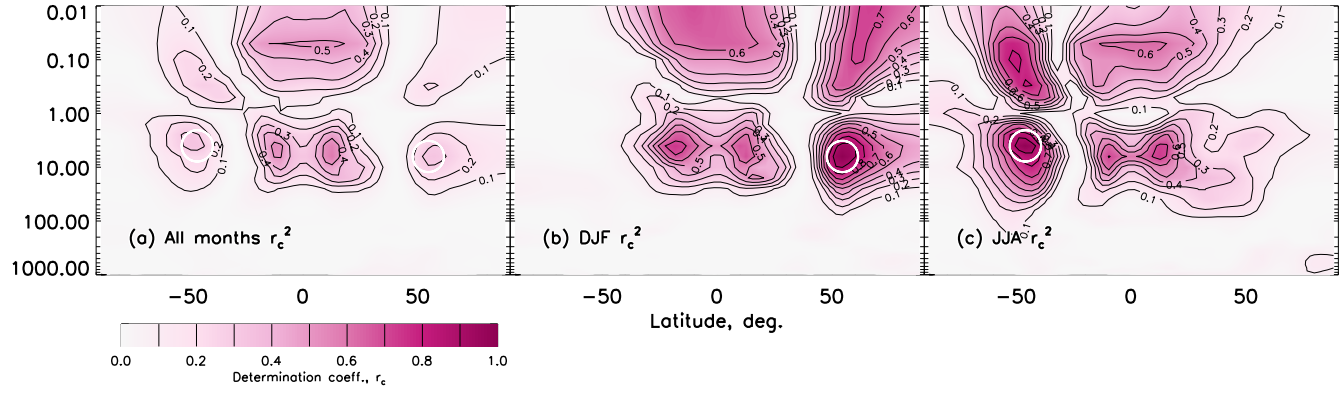

Figure 9. Coefficient of determination (R^2) maps of the mid-latitude stratosphere dynamical (MLSD) index with SOCOL model temperature at all latitudes and altitudes for (**a**) all months, (**b**) DJF and (**c**) JJA months. White circles represent the approximate region that the MLSD index is derived from.

In Fig. 9 we show the explanatory power of the MLSD index for nudged-model temperature anomalies everywhere (1983–2012), with the coefficient of determination r_c^2, or R^2, representing the amount of variation that the regressor can account for. It ranges from 0 to 1; a value of 1 is synonymous with the index accounting for 100% of the variability. In Fig. 9a the MLSD index can account for >50% of variability between 10 and 1 hPa, and above 0.05 hPa. Explanatory power at mid-latitudes is less (up to ∼30%), even at the index source locations (white circles), because the MLSD index has almost zero explanatory power half of the time there (see Fig. 8). In Fig. 9b and c, the MLSD index is shown to be good at explaining DJF/JJA variability: above 20 hPa it can account for over 70% of equatorial variability, more than 60% of polar mesospheric variability (80% in the SH), and much of polar stratosphere variability.

5 Improvement in MLR analysis using the MLSD index

The MLSD index leads to a large uncertainty reduction in MLR analysis. To show this, we consider MLR with or without the index. In both cases we use the six regressors mentioned in section 1, except we use the F30 radio flux as a proxy for solar variability, as this is superior to the F10.7 cm radio flux (Dudok de Wit et al., 2014). We do not consider use of any auto-regressive modelling. In Fig. 10a, we show the combined explanatory power, i.e. the total R^2 of all regressors, for 1983–2005 in SSU temperature observations (red), and JRA-55 (blue) and MERRA (yellow) reanalyses. R^2 without the MLSD index (dotted lines; Fig. 10a) shows that only about 50% (R^2=0.5) of the stratospheric variability above 10 hPa can be accounted for. However, with the MLSD index (solid lines) R^2 is >0.8 (MERRA ∼0.7) and, in all cases, the MLSD index peaks at ∼5 hPa with R^2 increasing by 0.4, or an absolute improvement of up to 40% (see negative values in the left panel of Fig. 10a, i.e. $R^2_{w/oMLSD}$-$R^2_{w/MLSD}$). In the right panel of Fig. 10a, we show the relative change in regressor uncertainty [($\sigma^2_{w/MLSD}$ - $\sigma^2_{w/oMLSD}$) / $\sigma^2_{w/oMLSD}$×100], where σ is based on the Student's t-test. The uncertainty estimates on the regressors decrease by up to ∼45% (SSU), ∼40% (JRA-55) and ∼35% (MERRA). In addition, the index increases R^2 above 0.4 hPa.

Atmos. Chem. Phys. Discuss., doi:10.5194/acp-2016-449, 2016
Manuscript under review for journal Atmos. Chem. Phys.
Published: 8 July 2016

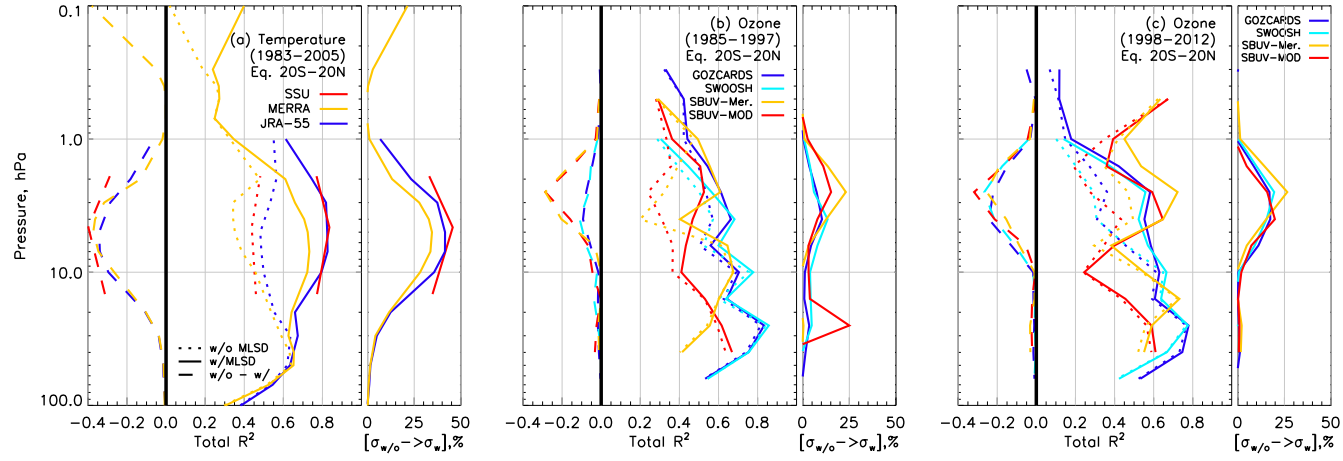

Figure 10. Coefficient of determination summed over all regressors (R_c^2) and the reduction in the Student's t-test-based error on regressor coefficients (%) for equatorial profiles (positive values) for (**a**) temperature from 1985–2005, and for ozone between (**b**) 1985 and 1997, and (**c**) 1998 and 2012 for various datasets (see legend). For R^2, dotted lines represent estimates without the MLSD index, solid lines with, and the difference (without-MLSD minus with-MLSD) is given as negative and dashed lines.

To show the MLSD index only improves the explanatory power, and does not alias with other regressors, we calculate the relative importance of each regressor without (blue in Fig. 11) and with (red) the MLSD index by decomposing R^2 (see Bi (2012) for a comprehensive review of this technique), which depends on the order regressors are considered, unless the regressors are orthogonal, which is usually not the case for the three decades we consider here (see e.g. Chiodo et al. (2014)). We use the robust LGM Measure (Lindeman et al., 1980), which determines relative importance by averaging over all possible, n!, ordering of regressors (720 for 6 regressors, 5040 for 7). In Fig. 11a we show the relative importance of each regressor, and the total, in explaining the variance in SSU temperature at 4.6 hPa; curves represent the complete distributions resulting from 10000 bootstrappings of every ordering. The MLSD index influences the relative importance of the other regressors very little, and therefore does not alias with them. At 4.6 hPa the MLSD index accounts for ∼41% of temperature variance and increases the total variance accounted for from 45% to 84% (peak values; solid white lines); we see similar results at the other two pressure levels (Fig. 11c). Fig. 11b shows that seasonal MLR analysis is enhanced: September-October-November (SON) months do not improve much (∼6%); March-April-May (MAM), JJA and DJF peaks increase by more than double the 68% confidence intervals, i.e. by an additional ∼15%, ∼15% and ∼20%, respectively.

Similar results are found for ozone. Figs. 10b and c shows the ozone composites (see section 2.2) split into 1985–1997 and 1998–2012 time periods, reflecting those often used to investigate ozone trends (e.g. Harris et al. (2015)). There are significant differences in R^2 between the ozone composites from the MLR analysis, which reflects the fact that different equatorial decadal trends are found between the ozone datasets (Tummon et al., 2015; Harris et al., 2015) and in solar signal profiles (Maycock et al., 2016) extracted with MLR (see also Fig. 13), which may be related to the way these composites of datasets have been merged together. While smaller for ozone than temperature, an improvement is found in explaining variance (R^2

Atmos. Chem. Phys. Discuss., doi:10.5194/acp-2016-449, 2016
Manuscript under review for journal Atmos. Chem. Phys.
Published: 8 July 2016

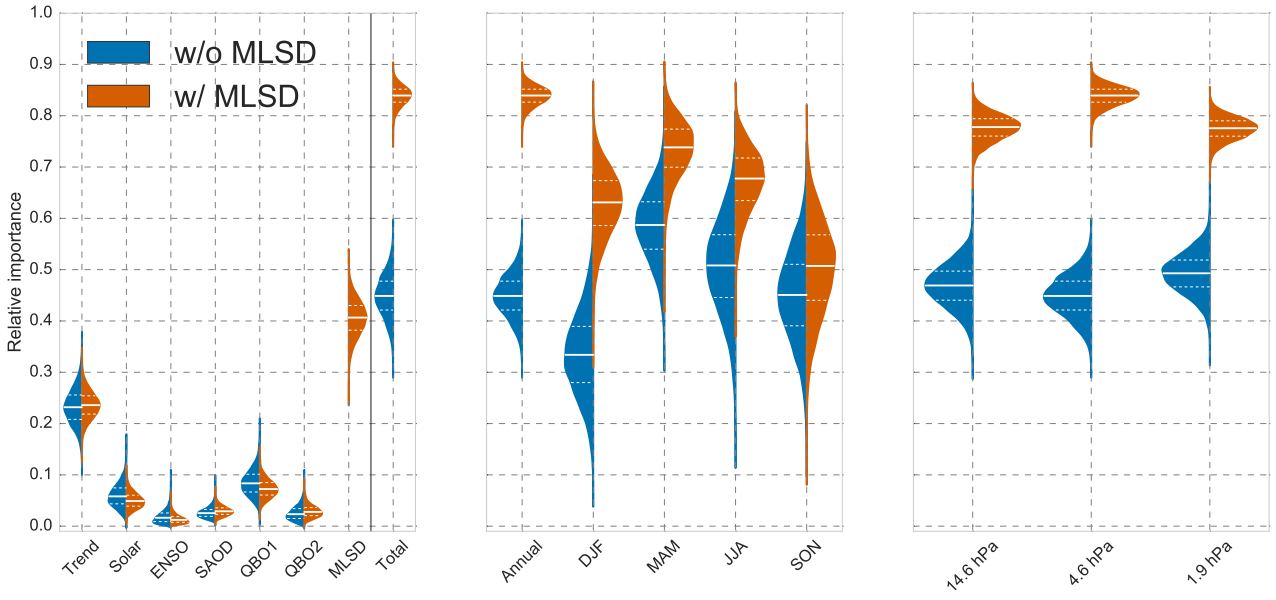

Figure 11. The full distributions of R^2 from MLR of SSU equatorial temperature (20S–20N, 1983–2005) without (blue) and with (red) the MLSD index showing: (**left**) 4.6 hPa R^2 values for all the regressors considered in the analysis and the total; (**middle**) the annual and seasonal total R^2 at 4.6 hPa; and (**c**) the annual total R^2 for the three SSU pressure levels. Distributions were calculated from 10000 bootstrapped samples for each of the possible (n=6) 720, or (n=7) 5040, order of regressors. Solid white lines are at the distribution peak, dotted lines are the 68% confidence intervals.

∼0.3), and errors reduce by up to ∼30% (smaller for SWOOSH and GOZCARDS pre-1998). Furthermore, Fig. 12 shows the relative importance of regressor, and the total, for all four ozone composites for the 1998-2012 period at 1.6 hPa. We use box-and-whisker plots to condense information: boxes and whiskers represent 68% and 95% confidence intervals around the peak (central line); diamonds are all remaining samples, so the full distribution is given. As for temperature, ozone regressors are not significantly influenced by the MLSD index (not shown). We see that at this pressure level, most of the variance is given by QBO2 and MLSD indices. In all four cases MLSD accounts for the same contribution to total variance (∼20%), within the 68% confidence intervals.

In Fig. 13, we show the equatorial decadal trend profiles of the datasets considered in Fig. 10 and the 2σ uncertainties derived from multiple linear regression with (thick lines) and without (thin lines) the MLSD index, between 25 and 0.2 hPa. A full discussion of the differences in the profiles is undertaken by Tummon et al. (2015) and Harris et al. (2015), so we do not repeat that here. We simply note that the mean decadal equatorial trends in temperature are almost unaffected by the MLSD index (right panel of Fig. 13). However, we see that the influence of the MLSD index on the mean profile of ozone, in each of the four cases presented here, leads to a decrease in the ozone trend of between ∼0.5–1% per decade (i.e. shaded region in Fig. 13), at the altitudes where the index also performs best at reducing uncertainties (left panel of Fig. 13). This decrease may be a result of the largest anomalies after 1998 being positive (see upper plot in Fig. 1), which might introduce a slight upward bias in the

Atmos. Chem. Phys. Discuss., doi:10.5194/acp-2016-449, 2016
Manuscript under review for journal Atmos. Chem. Phys.
Published: 8 July 2016

Atmospheric Chemistry and Physics Discussions

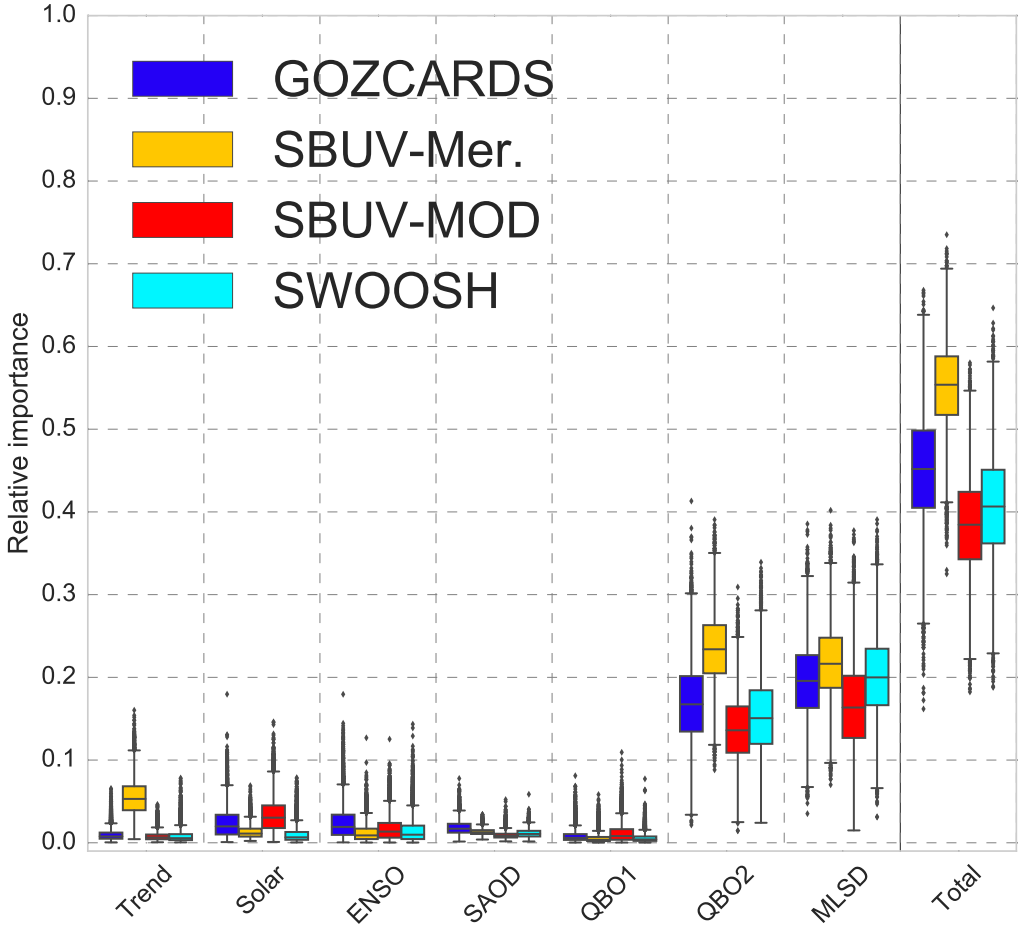

Figure 12. Box-and-whisker plots of the coefficient of determination (R^2) of each regressor, and the combined total, from multiple linear regression analysis of four ozone composite datasets at 1.6 hPa for 20S–20N and 1998–2012. The most-likely value is given by the central bar, the box represents 68% of the samples, the whisker 95% and diamonds all outliers. Distributions were calculated from 10000 bootstrapped samples of each of the possible 5040 regressor orderings.

trend analysis; once accounted for with the MLSD index, this bias is removed and the trend is reduced slightly. Nevertheless, this result suggests that ozone trend estimates that do not take the short, anomalous variability into account will overestimate the decadal trends, though it is clear that the biggest uncertainties remain in the underlying datasets themselves (Harris et al., 2015).

Atmos. Chem. Phys. Discuss., doi:10.5194/acp-2016-449, 2016
Manuscript under review for journal Atmos. Chem. Phys.
Published: 8 July 2016

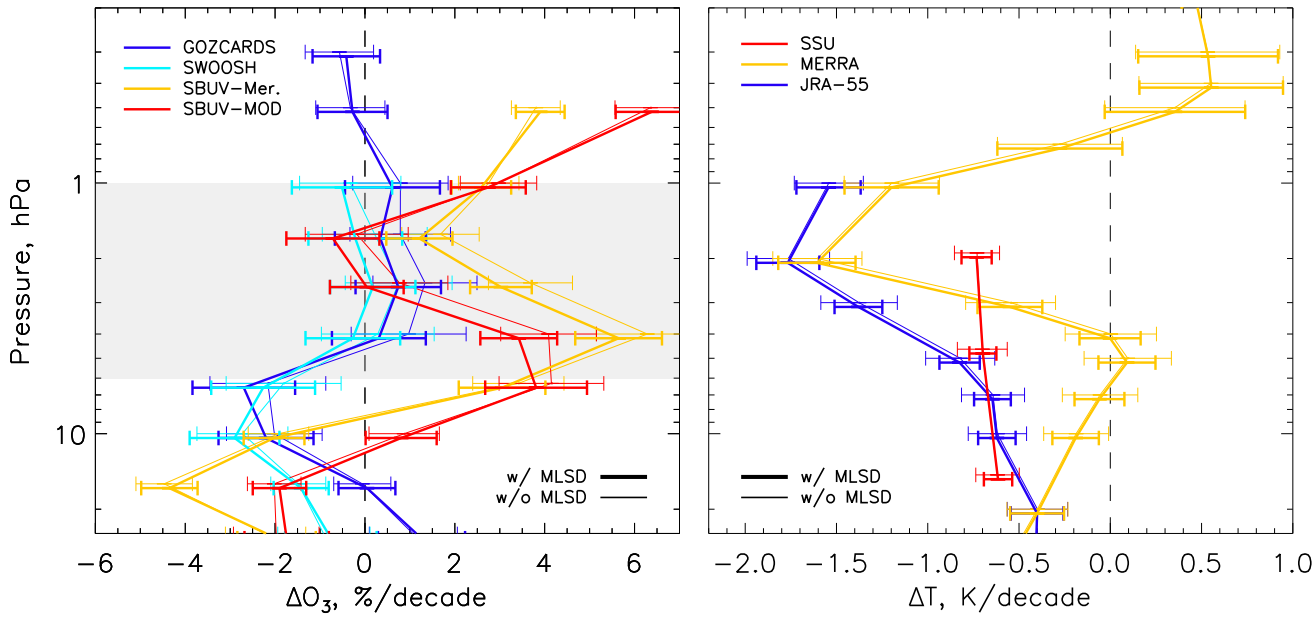

Figure 13. Equatorial stratospheric decadal trend profiles for (left) ozone between 1998 and 2012, and (right) for temperature between 1985 and 2005, for the datasets considered in Fig. 10. Thin lines represent profiles without the MLSD index, thick lines are with. Profiles with the MLSD index have been offset from the actual pressure levels for clarity.

6 Conclusions

We have shown that detrended and deseasonalised ozone and temperature anomalies in the tropics are strongly influenced by mid-latitude dynamical perturbations that influence temperature throughout the entire upper stratosphere and mesosphere of the perturbed hemisphere. The strongest correlations with these anomalies occur at latitudes around 50° in the winter of both hemispheres, which are linked to changes in wave-forcing.

We develop a new mid-latitude stratosphere dynamical (MLSD) index, which has the power to considerably improve the statistical significance of ozone and temperature trends, and explain much larger fractions of the total variability. Our results suggest that the index is able to improve the uncertainty of temperature and ozone estimates by up to 45 and 30%, respectively, between 0.3 and 6.3 hPa. While we focus on equatorial temperature and ozone, we suggest it could also be used in the analysis of other stratospheric variables, and also out of the equatorial region and in the mesosphere. The MLSD index should be employed in future investigations of stratospheric trends in the upper stratosphere and mesosphere. For modelling studies, this index can be extracted from pressure levels and latitudes similar to those put forward here, though the exact peak is likely to be model dependent; for future trends it may be necessary to determine the exact peak again since the regions of wave propagation and breaking may change.

Atmos. Chem. Phys. Discuss., doi:10.5194/acp-2016-449, 2016
Manuscript under review for journal Atmos. Chem. Phys.
Published: 8 July 2016

In all cases considered here, the MLSD index both improves our ability to reduce uncertainties and better explain equatorial stratospheric ozone and temperature variability and, by extension, will have the power to improve MLR analysis of stratospheric and mesospheric polar variability.

Acknowledgements. We thank David Thompson for helpful discussion and suggestions. We thank the GOZCARDS, SWOOSH and SBUV teams for their ozone products. We thank the Sounding of the Atmosphere using Broadband Emission Radiometry (SABER/TIMED) science team for their data. We acknowledge SATIRE-S data from http://www2.mps.mpg.de/ projects/sun-climate/data.html. W. T. Ball was funded by Swiss National Science Foundation (SNSF) grants 200021_149182 (SILA) and 200020_163206 (SIMA). T. Sukhodolov was funded by SNSF grant 200020_153302. A. Kuchar was funded by Charles University in Prague, No. 1474314; and Czech Science Foundation (GA CR), No. 16-01562J. E. V. Rozanov was partially funded by SNSF grant CRSII2_147659 (FUPSOL-II). F. Tummon thanks SNSF for funding. The National Center for Atmospheric Research is sponsored by the National Science Foundation.

Atmos. Chem. Phys. Discuss., doi:10.5194/acp-2016-449, 2016
Manuscript under review for journal Atmos. Chem. Phys.
Published: 8 July 2016

Atmospheric Chemistry and Physics Discussions

References

Ball, W. T., Haigh, J. D., Rozanov, E. V., Kuchar, A., Sukhodolov, T., Tummon, F., Shapiro, A. V., and Schmutz, W.: High solar cycle spectral variations inconsistent with stratospheric ozone observations, Nature Geoscience, 9, 206–209, doi:10.1038/ngeo2640, 2016.

Bi, J.: A review of statistical methods for determination of relative importance of correlated predictors and identification of drivers of consumer liking, Journal of Sensory Studies, 27, doi:10.1111/j.1745-459X.2012.00370.x, 2012.

Birner, T. and Bönisch, H.: Residual circulation trajectories and transit times into the extratropical lowermost stratosphere, Atmos. Chem. Phys., 11, 817–827, doi:10.5194/acp-11-817-2011, 2011.

Butchart, N.: The Brewer-Dobson circulation, Reviews of Geophysics, 52, 157–184, doi:10.1002/2013RG000448, 2014.

Charney, J. G. and Drazin, P. G.: Propagation of planetary-scale disturbances from the lower into the upper atmosphere, Journal of Geophysical Research, 66, 83–109, doi:10.1029/JZ066i001p00083, 1961.

Chen, W., Takahashi, M., and Graf, H.-F.: Interannual variations of stationary planetary wave activity in the northern winter troposphere and stratosphere and their relations to NAM and SST, Journal of Geophysical Research (Atmospheres), 108, 4797, doi:10.1029/2003JD003834, 2003.

Chiodo, G., Marsh, D. R., Garcia-Herrera, R., Calvo, N., and García, J. A.: On the detection of the solar signal in the tropical stratosphere, Atmospheric Chemistry & Physics, 14, 5251–5269, doi:10.5194/acp-14-5251-2014, 2014.

Chipperfield, M. P., Dhomse, S. S., Feng, W., McKenzie, R. L., Velders, G. J. M., and Pyle, J. A.: Quantifying the ozone and ultraviolet benefits already achieved by the Montreal Protocol, Nature Communications, 6, 7233, doi:10.1038/ncomms8233, 2015.

Davis, S. M., Rosenlof, K. H., Hassler, B., Hurst, D. F., Read, W. G., Vömel, H., Selkirk, H., Fujiwara, M., and Damadeo, R.: The Stratospheric Water and Ozone Satellite Homogenized (SWOOSH) database: A long-term database for climate studies, Earth Syst. Sci. Data Discuss., 10.5194/essd-2016-16, 1–59, 2016.

Dee, D. P., Uppala, S. M., Simmons, A. J., Berrisford, P., Poli, P., Kobayashi, S., Andrae, U., Balmaseda, M. A., Balsamo, G., Bauer, P., Bechtold, P., Beljaars, A. C. M., van de Berg, L., Bidlot, J., Bormann, N., Delsol, C., Dragani, R., Fuentes, M., Geer, A. J., Haimberger, L., Healy, S. B., Hersbach, H., Hólm, E. V., Isaksen, L., Kållberg, P., Köhler, M., Matricardi, M., McNally, A. P., Monge-Sanz, B. M., Morcrette, J.-J., Park, B.-K., Peubey, C., de Rosnay, P., Tavolato, C., Thépaut, J.-N., and Vitart, F.: The ERA-Interim reanalysis: configuration and performance of the data assimilation system, Quarterly Journal of the Royal Meteorological Society, 137, 553–597, doi:10.1002/qj.828, 2011.

Dudok de Wit, T., Bruinsma, S., and Shibasaki, K.: Synoptic radio observations as proxies for upper atmosphere modelling, Journal of Space Weather and Space Climate, 4, A06, doi:10.1051/swsc/2014003, 2014.

Ebita, A., Kobayashi, S., Ota, Y., Moriya, M., Kumabe, R. Onogi, K., Harada, Y., Yasui, S., Miyaoka, K., Takahashi, K., Kamahori, H., Kobayashi, C., Endo, H., Soma, M., Oikawa, Y., and Ishimizu, T.: The Japanese 55-year reanalysis (JRA-55): An Interim Report, Sola, 7, 2011.

Egorova, T., Rozanov, E., Gröbner, J., Hauser, M., and Schmutz, W.: Montreal Protocol Benefits simulated with CCM SOCOL, Atmospheric Chemistry & Physics, 13, 3811–3823, doi:10.5194/acp-13-3811-2013, 2013.

Frith, S. M., Kramarova, N. A., Stolarski, R. S., McPeters, R. D., Bhartia, P. K., and Labow, G. J.: Recent changes in total column ozone based on the SBUV Version 8.6 Merged Ozone Data Set, Journal of Geophysical Research (Atmospheres), 119, 9735–9751, doi:10.1002/2014JD021889, 2014.

Froidevaux, L., Anderson, J., Wang, H.-J., Fuller, R. A., Schwartz, M. J., Santee, M. L., Livesey, N. J., Pumphrey, H. C., Bernath, P. F., Russell, III, J. M., and McCormick, M. P.: Global OZone Chemistry And Related Datasets for the Stratosphere (GOZCARDS): methodology and sample results with a focus on HCl, H_2O, and O_3, Atmospheric Chemistry & Physics Discussions, 15, 5849–5957, doi:10.5194/acpd-15-5849-2015, 2015.

Garcia, R. R. and Randel, W. J.: Acceleration of the Brewer-Dobson Circulation due to Increases in Greenhouse Gases, Journal of Atmospheric Sciences, 65, 2731–2739, doi:10.1175/2008JAS2712.1, 2008.

García-Herrera, R., Calvo, N., Garcia, R. R., and Giorgetta, M. A.: Propagation of ENSO temperature signals into the middle atmosphere: A comparison of two general circulation models and ERA-40 reanalysis data, Journal of Geophysical Research (Atmospheres), 111, D06101, doi:10.1029/2005JD006061, 2006.

Haigh, J. D., Winning, A. R., Toumi, R., and Harder, J. W.: An influence of solar spectral variations on radiative forcing of climate, Nature, 467, 696–699, 2010.

Harris, N. R. P., Hassler, B., Tummon, F., Bodeker, G. E., Hubert, D., Petropavlovskikh, I., Steinbrecht, W., Anderson, J., Bhartia, P. K., Boone, C. D., Bourassa, A., Davis, S. M., Degenstein, D., Delcloo, A., Frith, S. M., Froidevaux, L., Godin-Beekmann, S., Jones, N., Kurylo, M. J., Kyrölä, E., Laine, M., Leblanc, S. T., Lambert, J.-C., Liley, B., Mahieu, E., Maycock, A., de Mazière, M., Parrish, A., Querel, R., Rosenlof, K. H., Roth, C., Sioris, C., Staehelin, J., Stolarski, R. S., Stübi, R., Tamminen, J., Vigouroux, C., Walker, K. A., Wang, H. J., Wild, J., and Zawodny, J. M.: Past changes in the vertical distribution of ozone - Part 3: Analysis and interpretation of trends, Atmospheric Chemistry & Physics, 15, 9965–9982, doi:10.5194/acp-15-9965-2015, 2015.

Haynes, P. H., McIntyre, M. E., Shepherd, T. G., Marks, C. J., and Shine, K. P.: On the 'Downward Control' of Extratropical Diabatic Circulations by Eddy-Induced Mean Zonal Forces., Journal of Atmospheric Sciences, 48, 651–680, doi:10.1175/1520-0469(1991)048<0651:OTCOED>2.0.CO;2, 1991.

Hitchcock, P., Shepherd, T. G., and Manney, G. L.: Statistical Characterization of Arctic Polar-Night Jet Oscillation Events, Journal of Climate, 26, 2096–2116, doi:10.1175/JCLI-D-12-00202.1, 2013.

Holton, J. R. and Mass, C.: Stratospheric Vacillation Cycles., Journal of Atmospheric Sciences, 33, 2218–2225, doi:10.1175/1520-0469(1976)033<2218:SVC>2.0.CO;2, 1976.

Holton, J. R., Haynes, P. H., McIntyre, M. E., Douglass, A. R., Rood, R. B., and Pfister, L.: Stratosphere-troposphere exchange, Reviews of Geophysics, 33, 403–439, doi:10.1029/95RG02097, 1995.

Krivova, N. A., Solanki, S. K., Fligge, M., and Unruh, Y. C.: Reconstruction of solar irradiance variations in cycle 23: Is solar surface magnetism the cause?, Astronomy & Astrophysics, 399, L1–L4, doi:10.1051/0004-6361:20030029, 2003.

Kuchar, A., Sacha, P., Miksovsky, J., and Pisoft, P.: The 11-year solar cycle in current reanalyses: a (non)linear attribution study of the middle atmosphere, Atmos. Chem. Phys., 15, 6879–6895, doi:10.5194/acp-15-6879-2015, 2015.

Kuroda, Y. and Kodera, K.: Variability of the polar night jet in the Northern and Southern Hemispheres, Journal of Geophysical Research, 106, 20 703–20 714, doi:10.1029/2001JD900226, 2001.

Lima, L. M., Alves, E. O., Batista, P. P., Clemesha, B. R., Medeiros, A. F., and Buriti, R. A.: Sudden stratospheric warming effects on the mesospheric tides and 2-day wave dynamics at 7degS, Journal of Atmospheric and Solar-Terrestrial Physics, 78, 99–107, doi:10.1016/j.jastp.2011.02.013, 2012.

Lindeman, R. H., Merenda, P. F., and Gold, R. Z.: Introduction to Bivariate and Multivariate Analysis, Scott Foresman & Co, 1980.

Maycock, A., Matthes, K., Tegtmeier, S., Thieblemont, R., and Hood, L.: The representation of solar cycle signals in stratospheric ozone - Part 1: A comparison of satellite observations, Atmos. Chem. Phys. Discuss., in review, doi:10.5194/acp-2015-882, 2016.

Nath, O. and Sridharan, S.: Equatorial middle atmospheric chemical composition changes during sudden stratospheric warming events, Atmospheric Chemistry & Physics Discussions, 15, 23 969–23 988, doi:10.5194/acpd-15-23969-2015, 2015.

Rienecker, M. M., Suarez, M. J., Gelaro, R., Todling, R., Bacmeister, J., Liu, E., Bosilovich, M. G., Schubert, S. D., Takacs, L., Kim, G.-K., Bloom, S., Chen, J., Collins, D., Conaty, A., da Silva, A., Gu, W., Joiner, J., Koster, R. D., Lucchesi, R., Molod, A., Owens, T., Pawson, S., Pegion, P., Redder, C. R., Reichle, R., Robertson, F. R., Ruddick, A. G., Sienkiewicz, M., and Woollen, J.: MERRA: NASA's Modern-Era Retrospective Analysis for Research and Applications, Journal of Climate, 24, 3624–3648, doi:10.1175/JCLI-D-11-00015.1, 2011.

Russell, J. M., Mlynczak, M. G., Gordley, L. L., Tansock, J. J., and Esplin, R. W.: Overview of the SABER experiment and preliminary calibration results, in: Optical Spectroscopic Techniques and Instrumentation for Atmospheric and Space Research III, edited by Larar, A. M., vol. 3756 of *Proc. SPIE*, pp. 277–288, 1999.

Shapiro, A. V., Rozanov, E. V., Shapiro, A. I., Egorova, T. A., Harder, J., Weber, M., Smith, A. K., Schmutz, W., and Peter, T.: The role of the solar irradiance variability in the evolution of the middle atmosphere during 2004-2009, Journal of Geophysical Research (Atmospheres), 118, 3781–3793, doi:10.1002/jgrd.50208, 2013.

Shepherd, M. G., Wu, D. L., Fedulina, I. N., Gurubaran, S., Russell, J. M., Mlynczak, M. G., and Shepherd, G. G.: Stratospheric warming effects on the tropical mesospheric temperature field, Journal of Atmospheric and Solar-Terrestrial Physics, 69, 2309–2337, doi:10.1016/j.jastp.2007.04.009, 2007.

Solomon, S.: Stratospheric ozone depletion: A review of concepts and history, Reviews of Geophysics, 37, 275–316, doi:10.1029/1999RG900008, 1999.

Soukharev, B. E. and Hood, L. L.: Solar cycle variation of stratospheric ozone: Multiple regression analysis of long-term satellite data sets and comparisons with models, Journal of Geophysical Research (Atmospheres), 111, D20314, doi:10.1029/2006JD007107, 2006.

Sridharan, S., Sathishkumar, S., and Gurubaran, S.: An unusual reduction in the mesospheric semi-diurnal tidal amplitude over Tirunelveli (8.7degN, 77.8degE) prior to the 2011 minor warming and its relationship with stratospheric ozone, Journal of Atmospheric and Solar-Terrestrial Physics, 89, 27–32, doi:10.1016/j.jastp.2012.07.012, 2012.

Stenke, A., Schraner, M., Rozanov, E., Egorova, T., Luo, B., and Peter, T.: The SOCOL version 3.0 chemistry-climate model: description, evaluation, and implications from an advanced transport algorithm, Geoscientific Model Development, 6, 1407–1427, doi:10.5194/gmd-6-1407-2013, 2013.

Stolarski, R. S., Douglass, A. R., Remsberg, E. E., Livesey, N. J., and Gille, J. C.: Ozone temperature correlations in the upper stratosphere as a measure of chlorine content, Journal of Geophysical Research (Atmospheres), 117, D10305, doi:10.1029/2012JD017456, 2012.

Tummon, F., Hassler, B., Harris, N. R. P., Staehelin, J., Steinbrecht, W., Anderson, J., Bodeker, G. E., Bourassa, A., Davis, S. M., Degenstein, D., Frith, S. M., Froidevaux, L., Kyrölä, E., Laine, M., Long, C., Penckwitt, A. A., Sioris, C. E., Rosenlof, K. H., Roth, C., Wang, H.-J., and Wild, J.: Intercomparison of vertically resolved merged satellite ozone data sets: interannual variability and long-term trends, Atmospheric Chemistry & Physics, 15, 3021–3043, doi:10.5194/acp-15-3021-2015, 2015.

Wild, J. D. and Long, C. S.: A Coherent Ozone Profile Dataset from SBUV, SBUV/2: 1979 to 2013, in preparation, 2016.

WMO: Scientific Assessment of Ozone Depletion: 1994, Global Ozone Research and Monitoring Project, 37, 1994.

WMO: Scientific Assessment of Ozone Depletion: 2010, Global Ozone Research and Monitoring Project, 52, 516, 2011.

WMO: Scientific Assessment of Ozone Depletion: 2014 Global Ozone Research and Monitoring Project Report, World Meteorological Organization, p. 416, geneva, Switzerland, 2014.

Atmos. Chem. Phys. Discuss., doi:10.5194/acp-2016-449, 2016
Manuscript under review for journal Atmos. Chem. Phys.
Published: 8 July 2016

Yeo, K. L., Krivova, N. A., Solanki, S. K., and Glassmeier, K. H.: Reconstruction of total and spectral solar irradiance from 1974 to 2013 based on KPVT, SoHO/MDI, and SDO/HMI observations, Astronomy & Astrophysics, 570, A85, doi:10.1051/0004-6361/201423628, 2014.

Zou, C.-Z., Qian, H., Wang, W., Wang, L., and Long, C.: Recalibration and merging of SSU observations for stratospheric temperature trend studies, Journal of Geophysical Research (Atmospheres), 119, 13, doi:10.1002/2014JD021603, 2014.

Zubov, V., Rozanov, E., Egorova, T., Karol, I., and Schmutz, W.: Role of external factors in the evolution of the ozone layer and stratospheric circulation in 21st century, Atmospheric Chemistry & Physics, 13, 4697–4706, doi:10.5194/acp-13-4697-2013, 2013.